

Chemical composition of B-type supergiants in the OB 8, OB 10, OB 48, OB 78 associations of M 31

C. Trundle^{1,2}, P. L. Dufton¹, D. J. Lennon², S. J. Smartt³, and M. A. Urbaneja⁴

¹ The Department of Pure and Applied Physics, The Queen's University of Belfast, Belfast BT7 1NN, Northern Ireland

² The Isaac Newton Group of Telescopes, Apartado de Correos 321, 38700, Santa Cruz de La Palma, Canary Islands, Spain

³ Institute of Astronomy, University of Cambridge, Madingley Road, Cambridge, CB3 0HA, USA

⁴ Institutio de Astrofísica de Canarias, 38200 La Laguna, Tenerife, Spain

Received 23 April 2002 / Accepted 15 July 2002

Abstract. Absolute and differential chemical abundances are presented for the largest group of massive stars in M 31 studied to date. These results were derived from intermediate resolution spectra of seven B-type supergiants, lying within four OB associations covering a galactocentric distance of 5–12 kpc. The results are mainly based on an LTE analysis, and we additionally present a full non-LTE, unified model atmosphere analysis of one star (OB 78-277) to demonstrate the reliability of the differential LTE technique. A comparison of the stellar oxygen abundance with that of previous nebular results shows that there is an offset of between ~ 0.15 – 0.4 dex between the two methods which is critically dependent on the empirical calibration adopted for the R_{23} parameter with $[O/H]$. However within the typical errors of the stellar and nebular analyses (and given the strength of dependence of the nebular results on the calibration used) the oxygen abundances determined in each method are fairly consistent. We determine the radial oxygen abundance gradient from these stars, and do not detect any systematic gradient across this galactocentric range. We find that the inner regions of M 31 are not, as previously thought, very “metal rich”. Our abundances of C, N, O, Mg, Si, Al, S and Fe in the M 31 supergiants are very similar to those of massive stars in the solar neighbourhood.

Key words. galaxies: individual: M 31

1. Introduction

Until recently studies of the spatial distribution of chemical species in M 31 and many other external galaxies mainly involved H II regions and supernovae remnants (SNR's) (see for example: Dennefeld & Kunth 1981; Blair et al. 1982; Galarza et al. 1999). In M 31, the H II regions have low excitation, thus the [O III] lines used in estimating the electron temperature are often too weak to be detected. Without a direct method of determining the electron temperature, empirical calibrations must be implemented and in some cases extrapolated to estimate abundances of these H II regions. Depending on the empirical calibrations adopted significantly different abundance estimates are derived (Pagel et al. 1980; Mc Gaugh 1991; Zaritsky et al. 1994; Kobulnicky et al. 1999; Pilyugin 2000, 2001a, 2001b). This indicates that an independent method of evaluating the abundance gradients of external galaxies is needed. Blue supergiants are amongst the optically brightest stellar objects in spiral and irregular galaxies, and can provide us with such a method.

Previous studies have shown that quantitative spectroscopy of B-type supergiants in Local Group galaxies can be carried

out successfully using 4 m telescopes (see Monteverde et al. 2000; Smartt et al. 2001b). The added advantage of using blue supergiants over H II regions is that their rich metal line optical spectra provide us with a means of studying elements not observed in the emission line spectra of H II regions. Other than H, He and CNO, some α -processed and Fe-peak elements are observed in the spectrum of blue supergiants. These elements are important as they help to put constraints on nucleosynthesis theories and models of the chemical evolution of galaxies.

Studies of blue supergiants in external galaxies can also help to enhance the use of the Period-Luminosity (PL) relationship of Cepheid variables in two ways. First one can determine *stellar* abundances in the fields where Cepheids are found to constrain the effect of metallicity on the PL relation. Secondly, although it is difficult to determine extinction to Cepheids themselves model atmosphere fits can accurately determine the interstellar extinction towards blue supergiants, and hence determine reddening in stellar fields where Cepheids are found. In addition, it now appears possible that blue supergiants could be used to determine extragalactic distances by a properly calibrated independent technique, using the wind momentum-luminosity relationship (WLR, see Puls et al. 1996; Kudritzki et al. 1999; Kudritzki & Puls 2000). The WLR allows

Send offprint requests to: C. Trundle, e-mail: ct@ing.iac.es

Table 1. Observational details for the M 31 targets. The OB-association numbers are from van den Bergh (1964), while the stellar identifications are from Massey et al. (1986). For example OB 8-17 is star number 17 in association 8. The alternative identifications are from Berkhuijsen et al. (1988). Visual magnitudes and spectral types are taken from Massey et al. (1995) – the latter are identified by the authors initials, MAPPW. Also listed are the spectral types and heliocentric radial velocities, v_r (in km s^{-1}), estimated from our spectra as discussed in Sects. 2 and 3. The data for OB 10-64 have been previously discussed by Smartt et al. (2001b).

Star name	Alternative ID	V	Spectral Type		Time (hours)	S/N ratio	v_r
			MAPPW	Here			
OB 8-17	41-2178	18.01	O9-B1I	B1Ia	4.0	50	-102 ± 10
OB 8-76		18.52	B0III	B0.5Ia	4.0	30	-34 ± 7
OB 10-64	41-2265	18.10	B1I	B0Ia	4.5	50	-113 ± 11
OB 48-234		18.50	B1I	B1.5Ia	2.5	30	-125 ± 8
OB 48-358		18.70	B0-1I	B0Ia	2.5	30	-107 ± 22
OB 78-159	40-1876	17.97	B0I	B0Ia	7.0	40	-467 ± 20
OB 78-277	40-1939	17.35	B1I	B1.5Ia	7.0	65	-567 ± 9
OB 78-478	40-2028	17.50	B0-1I	B1.5Ia	5.0	55	-561 ± 12

distances to be determined via detailed studies of the radiatively driven winds in O, B and A-type supergiants. Several of the stars that will be presented here have been observed by HST with both WFPC2 and STIS, in a broader project to use them as calibrators of the WLR within the Local Group. First steps in this has occurred by measuring the terminal velocities from the UV STIS spectra in a related paper (Bresolin et al. 2002). However to carry out the WLR study in full the atmospheric parameters and chemical composition of the early-type supergiants must be reliably estimated, and this is the focus of this paper.

Previous to this work, the largest homogeneous abundance analysis on a set of supergiants in M 31 is that by Venn et al. (2000 – hereafter VMLPKL). In this study, two A-type supergiants and one F-type supergiant were analysed using high resolution spectra from the Keck 10 m telescope and the HIRES spectrograph. The stellar oxygen abundances in this analysis suggested a shallow or negligible abundance gradient in M 31. The nebular H II regions give abundance gradients in the range of -0.013 – -0.027 dex kpc^{-1} , depending on the empirical calibration used, however the VMLPKL results were based around only three stars and the individual abundances are reasonably consistent to H II region results at similar galactocentric distances. Definite conclusions from three points are not warranted, and our experience should caution us against the use of restricted datasets in determining stellar abundance gradients e.g. see the discussion of Smartt & Rolleston (1997) on the abundance gradient in the Milky Way. Additionally Smartt et al. (2001b) have analysed a B0Ia supergiant, OB 10-64, in the inner regions of M 31 and compared it to the abundances derived in the H II region surrounding the OB 10 association. The absolute nebular abundance is critically dependent on which calibration of the R_{23} parameter is used, however there is good agreement between the stellar and at least one parameterization of the nebular result.

Here we present a spectroscopic analysis for the largest sample of supergiants in M 31 considered to date and covering a range in galactocentric distance of 5–12 kpc. The elemental abundances of these B-type supergiants are presented and their reliability discussed including the uncertainties incurred by

adopting an LTE analysis. We also determine the oxygen abundance gradient in M 31 and compare it with that determined from H II regions and A & F-type supergiants (VMLPKL).

2. Observational data

The double armed spectrometer ISIS on the William Herschel Telescope was used to observe all the M 31 stars during two separate observing runs covering the nights 8–11 October 1997 and 28–29 September 1998 and exposure times are summarized in Table 1. The targets designations are taken from Massey et al. (1986), with alternative identifications from Berkhuijsen et al. (1988) being given when available. The spectrograph slit was positioned so that, if possible it included two targets within a particular OB association.

The spectra presented here were obtained using only the blue arm of the spectrograph (which was fed with a beam folding mirror) with the R1200B grating and a EEV42-80 CCD (with format 4096×2048 $13.5 \mu\text{m}$ pixels). A slit width of 1 arcsec was used giving a spectral resolution of $0.46 \text{ \AA}/\text{pixel}$. Although ISIS is a dual beam spectrometer with the ability to gather simultaneous red and blue spectra, the dichroic beam splitter introduces additional structure into the blue spectra and reduces the throughput of this arm. These ripples seriously compromise the quality of stellar absorption line spectra, and hence we chose only to observe in the blue. Spectra in the red region have been taken at the Keck telescope and a full wind analysis of the H α region will be presented elsewhere. The most important lines for a *photospheric* analysis lie in the blue which is the focus of this paper.

In Table 1, the total exposure times are listed and as conditions varied significantly during the two observing runs, the corresponding signal-to-noise ratio near to the central wavelength of the blue spectra are also given. Subsequently service spectroscopy was obtained for Galactic supergiants covering a range of spectral types from approximately B0Ia to B3Ia and these are summarized in Table 2. The instrumental setup was identical to that used for the M 31 targets with a mirror feeding the blue arm of the spectrograph – signal-to-noise ratios in the

reduced spectra were always in excess of 200 for these bright comparison stars.

The CCD frames were reduced to wavelength calibrated spectra using the IRAF reduction system¹. Standard procedures were used to bias correct and flat field the stellar images. As our targets are in young clusters, there was often considerable background Balmer line emission from the nebular regions surrounding the hot stars, which can vary over small spatial scales along the slit. Our spectral resolution is easily high enough that the important wings of H δ and H γ will be unaffected by the background nebulosity. However there may be residual errors in the cores of the stellar Balmer line profiles and less weight was given to modelling the line cores in the analysis. The spectra were wavelength calibrated using Cu-Ne & Cu-Ar lamp exposures that interleaved the stellar spectra. Individual stellar exposures were then cross-correlated to search for significant wavelength shifts – none were identified. The spectra were then combined using SCOMBINE and a variety of rejection criteria such as rejecting pixels with counts very high/low above/below the median; these were found to have little effect on the final spectra.

The spectra were transferred to the STARLINK spectrum analysis program DIPSO (Howarth et al. 1996) for subsequent analysis. This included estimating the stellar radial velocities and equivalent widths. Firstly metal line absorption features were identified in the spectra of the M 31 targets. For marginal features, the spectrum of a suitable Galactic comparison star (see Sect. 3) was used as a template and guide. The equivalent widths of the features were then estimated in both stars by non-linear least squares fitting of single or multiple Gaussian absorption profiles to normalised spectra. Normally both the positions and widths of the Gaussian profiles were allowed to vary. For the equivalent width estimates, the relative wavelength separations of lines within multiplets were fixed, while for marginal features in the M 31 targets, the widths were set to the mean value found for well observed lines. Further details of these procedures can be found in Smartt et al. (1996a). In the case of OB 10-64, the equivalent widths were taken from Smartt et al. (2001b).

For the radial velocity determinations, a common set of ten relatively strong, isolated metal and helium lines were adopted. For the M 31 targets, the radial velocities, transformed to a heliocentric frame are listed in Table 1. The error estimates are the sample standard deviation and if the errors are normally distributed the uncertainty in the mean should be approximately a factor of three smaller. The range in these error estimates probably reflects the variations in the data quality and intrinsic line strengths of the spectra.

Radial velocities of the OB 48 stars and the OB 78 stars, OB 78-277 & OB 78-478, agree within 10% of the radial velocities determined by Rubin & Ford (1970) for H II regions in the relevant OB associations. OB 78-159 has a radial velocity significantly less than that expected from a star situated in the OB 78 association. From WFPC2 images, taken

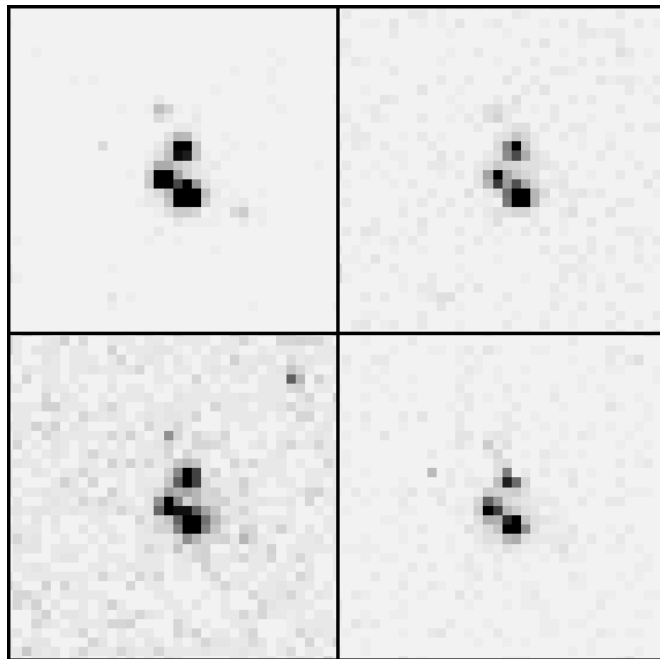


Fig. 1. WFPC2 images of OB 78-159. These images were taken in the filters $U - B - I - V$ starting upper left and going clockwise. These images show that OB 78-159 is a part of a multiple system with at least 3 components. The size of each image is 4×4 arcsecs.

in the U , B , V and I filters, OB 78-159 was observed to be part of a multiple system (see Fig. 1; from McCarthy et al. in preparation), which might explain the difference in radial velocity. An additional discrepancy is the large difference in the radial velocities of the OB 8 supergiants. No radial velocities have been measured for H II regions in OB 8, but from a neutral hydrogen mapping of M 31's velocity field the radial velocity in the region of the OB 8 association is expected to be $-140 \pm 10 \text{ km s}^{-1}$ (Unwin 1983). Furthermore, the OB 10 association lies in close proximity to OB 8 and the radial velocity of OB 10-64 is $-113 \pm 11 \text{ km s}^{-1}$ (see Table 1). Hence the radial velocity of OB 8-17 agrees well with what we expect for a genuine single member of the OB 8 association. The radial velocity for OB 8-76 differs by some 70 km s^{-1} which could suggest the star is part of a binary system, or has a peculiar velocity within the OB association. Being part of a binary does not necessarily exclude using the star in a detailed model atmosphere analysis as the companion may contribute little or no flux at these wavelengths, however it is an anomaly that should be kept in mind during the analysis. Radial velocities were also estimated for the comparison stars, the error estimates in this case being smaller and typically $\pm 5 \text{ km s}^{-1}$.

3. Spectral types for the M 31 targets

From our spectra, we have estimated spectral types. Given the relatively high spectral resolution and signal-to-noise, we expect that these may be more reliable than those deduced previously. Additionally this procedure will assist the identification of standards that will be suitable for a differential model atmosphere analysis.

¹ IRAF is written and supported by the IRAF programming group at the National Optical Astronomy Observatories (NOAO) in Tucson (<http://iraf.noao.edu>).

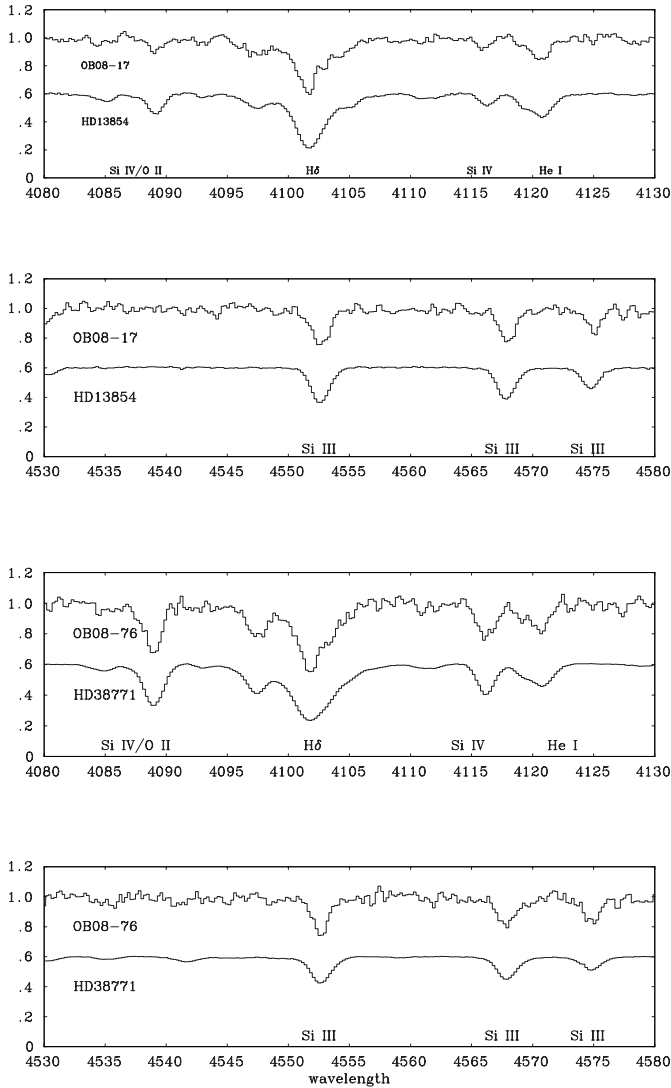


Fig. 2. Spectra of selected wavelength regions in two M 31 targets, OB 8-17 and OB 8-76. The spectra show lines of Si III and Si IV and the Balmer H_δ line; the former vary with effective temperature and the latter with surface gravity. Also shown are the spectra of two Galactic supergiants, HD 13854 (B1Iab) and HD 38771 (B0.5Ia), which appear to have similar spectral types.

For each of our M 31 targets, our initial approach was to attempt to identify a standard with both a similar hydrogen line spectrum (which constrains the luminosity class) and helium and metal line spectra (which constrains the spectral type). The latter criterion implicitly assumes that both the M 31 targets and the standards have similar chemical composition. For some of our M 31 targets, the metal line spectra appeared to be weak (possibly implying lower metal abundances) and here we have used the hydrogen and helium spectra and the *relative* strength of the metal lines. This is analogous to the procedures used by Lennon (1997) to estimate revised spectral types for SMC supergiants. The individual stars are discussed below:

OB 8-17: The observed spectra for this star has a relatively high S/N ratio and, besides lines of neutral helium and hydrogen, has a well developed metal line spectra. Comparison with the standard star spectra showed good agreement for B1Ia

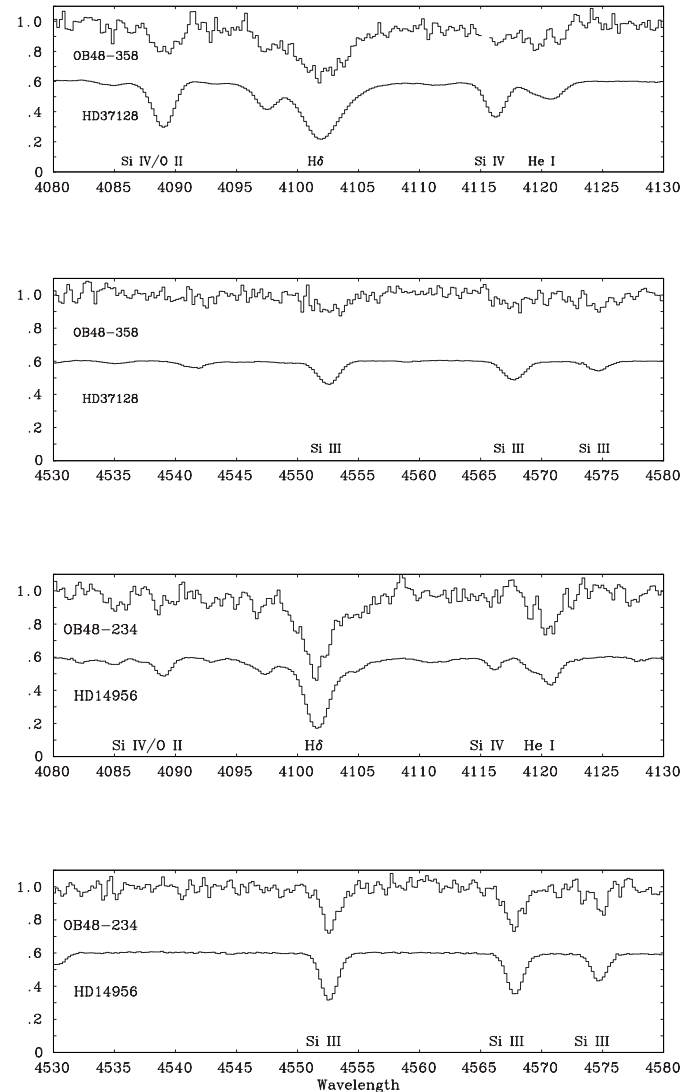


Fig. 3. As for Fig. 2, however the spectra are of the two M 31 targets OB 48-358 and OB 48-234 and the two Galactic supergiants, HD 14956(B1.5Ia) and HD 37128(B0Ia).

and B1.5Ia, with the former being probably superior. Selected regions of its observed spectra and that of the standard, HD 13854, are shown in Fig. 2.

OB 8-76: This star would appear to be hotter than OB 8-17, although the He II lines are not present in the observed spectrum. Good agreement is found with the spectrum of HD 38771 (B0.5Ia) and this is again illustrated in Fig. 2. The spectrum of HD 38771 may show a very weak He II line at 4686 Å but numerical simulations indicate that this would not have been observable at the S/N ratio of the OB 8-76 spectrum. Caution must be taken in adopting this spectral type due to the possibility of OB 8-76 being a composite star.

OB 10-64: The spectral type of this star is B0Ia and is discussed in Smartt et al. (2001b).

OB 48-358: Again this star would appear to be hotter than the other target in the cluster. This leads to the He I and Si III spectra being relatively weak as can be seen in Fig. 3. From the hydrogen and diffuse helium lines, HD 37128 would

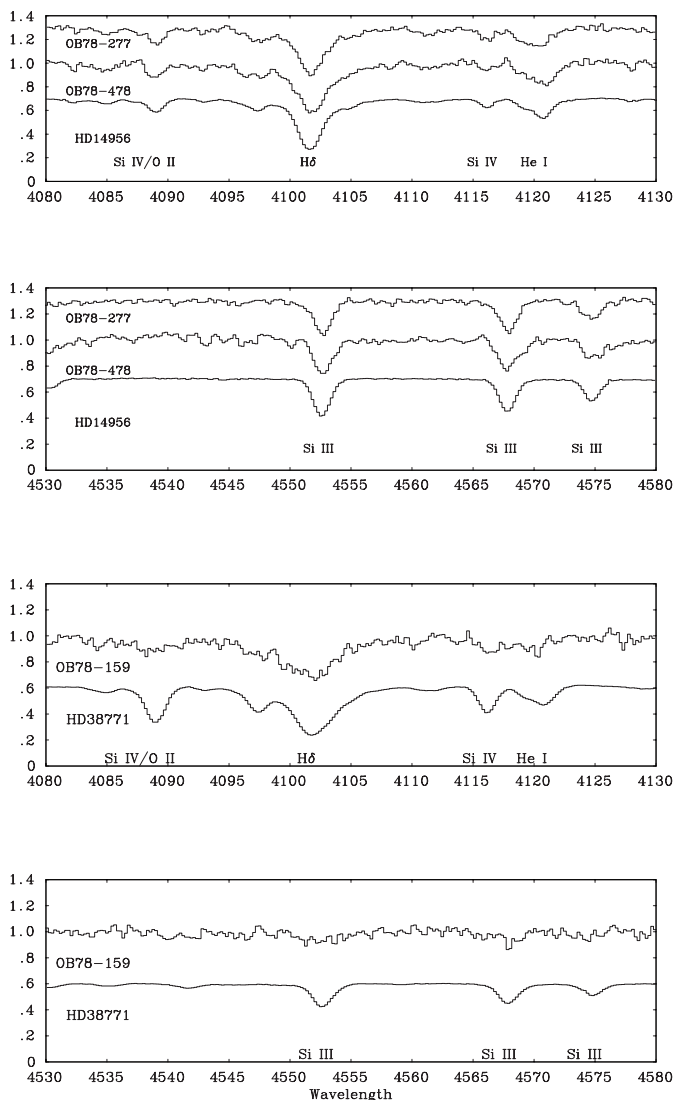


Fig. 4. As for Fig. 2, however the spectra are of three M 31 targets – two relatively cool (OB 78-277 and OB 78-478) and one relatively hot (OB 78-159). The two Galactic supergiants are HD 14956 (B1.5Ia) and HD 38771 (B0Ia).

appear similar, although we emphasize that the spectral type assignment may be subject to error.

OB 48-234: The spectra of both the OB 48 targets appear to have weaker metal line spectra than those of their Galactic counterparts. In turn this, coupled with the relatively poor quality of the spectra, makes the assignment of spectral types more difficult. In Fig. 3, the spectrum of OB 48-234 is compared with that of the standard HD 14956 (B1.5Ia). There is reasonable agreement for the hydrogen and neutral helium lines but the silicon spectra is weaker in the former – with the identification of the Si IV lines being marginal. Indeed a later spectral-type, such as B2Ia, would also be compatible with the data.

OB 78-277 and OB 78-478: These two M 31 targets are considered together as they have similar spectra, corresponding to spectral types of B1-2Ia. Indeed both spectra match well that of the Galactic standard HD 14956 (B1.5Ia) as can be seen

from Fig. 4. They have therefore been assigned identical spectral types.

OB 78-159: This star appears to be hotter than the other two targets in the association. However surprisingly its silicon spectrum appears to be significantly weaker than its Galactic counterparts – see Fig. 4. This behaviour is different to that found for both OB 78-277 and OB 78-478, which are presumably relatively nearby objects. The weak metal line spectrum makes the assignment of a spectral type more difficult for OB 78-159 but on the basis of the hydrogen and helium lines (including the absence of identifiable He II lines) a spectral type near B0Ia would appear appropriate. Moreover OB 78-159 appears to be part of a multiple system (see Fig. 1) with three distinct point sources resolved by HST, each of similar brightness in the *B*-band. Hence the spectra is a composite of these three sources and is not a single, B-type supergiant. It will not be considered further for detailed analysis.

Two general comments can be made about the spectral-type assignments. Firstly, there is relatively good agreement between our spectral types and those of Massey et al. (1995), although we are normally able to assign specific luminosity classes and to narrow the range of possible spectral types to one subgroup (i.e. B0, B1 or B2) – this is not surprising given the much higher spectral resolution and *S/N* ratios of our spectra. Secondly, the stars would appear to fall into two groups, five targets (OB 8-17, OB 8-76, OB 10-64, OB 78-277 and OB 78-478), which have similar silicon line strengths to their Galactic counterparts and two (OB 48-234 and OB 48-358), where the silicon spectra are significantly weakened. It is plausible to identify these differences as reflecting different metallicities in the stellar atmospheres and in turn, in the interstellar material from which they were formed. Indeed, considering the galactocentric distance of these associations (see Table 4), the different metallicities would be consistent with a decreasing radial gradient. We notice that OB 78-159 has a weaker silicon spectra than its standard and the other OB 78 stars. However this does not imply that the OB 78 association has varying metallicity but is probably due to OB 78-159 being a composite (see Sect. 4.2). We have also checked the HST WFPC2 images of the OB 48 and OB 78 associations which are available and the stars OB 48-234, OB 48-358, OB 78-277 and OB 48-478 all appear to be single point sources at this resolution. Photometry of these stars will be presented in a future paper (McCarthy et al., in preparation). In addition both OB 8-17 and OB 10-64 have been observed by STIS (Bresolin et al. 2002), and the HST acquisition images again show these are single point-like objects. Hence in the sample considered here, we have only one object (OB 8-76) which has not been confirmed as a single object at HST’s spatial resolution (at a distance of 783 kpc, 0.1'' corresponds to 0.4 pc in M 31).

4. LTE model atmosphere and abundance analyses

All the M 31 targets are luminous supergiants and as, for example, discussed by McErlean et al. (1999 - hereafter MLD) their spectra will be affected by significant non-LTE effects. However MLD also showed that even with a non-LTE

approach based on plane-parallel models without line-blanketing and stellar winds, it was difficult to obtain reliable *absolute* atmospheric parameters and abundances. Hence we will initially adopt a simple approach and use differential LTE methods. This will inevitably lead to the estimates of the atmospheric parameters and absolute chemical composition having significant uncertainties. However provided the M 31 targets are well matched (in terms of their atmospheric parameters) to the Galactic standards, differences in atmospheric parameters and chemical compositions should be more reliably estimated. In Sect. 5, we will carry out non-LTE calculations and discuss the effects departure from LTE conditions has on the differential abundances of these supergiants.

4.1. Atmospheric parameters

The LTE methods employed are similar to those described in Smartt et al. (1996b) and Rolleston et al. (1997), where more details can be found. All results are based on the grid of unblanketed LTE model atmospheres generated using the code TLUSTY (Hubeny 1988). This grid covered a range in effective temperatures of $10\,000 \leq T_{\text{eff}} \leq 35\,000$ and included logarithmic surface gravities from $\log g = 4.5$ down to near the Eddington stability limit. LTE line formation codes were then used to derive line profiles and equivalent widths leading to estimates of atmospheric parameters and chemical compositions.

Although this approach appears to be attractive, for evolved stars it has one major disadvantage. This is that it implicitly assumes that the chemical composition of the standard is representative of that of the Galactic ISM. However for supergiants, surface chemical compositions may be affected by material mixed from the stellar core that has been processed by nuclear reactions. Indeed MLD found evidence that the nitrogen and carbon abundances could be significantly modified by such mixing. Hence we will use non-LTE techniques in Sect. 5 to attempt to estimate more reliable absolute parameters for our M 31 targets.

The atmospheric parameters were initially estimated from the Si III/Si IV ionisation balance and the fitting of hydrogen line profiles to the observed spectra. The former principally constrains the effective temperature and the latter, the surface gravity. It is important to note that these effective temperatures are derived from unblanketed model atmospheres which may affect the ionisation balance and hence the absolute abundances. In order to derive highly accurate *absolute* abundances line-blanketed model should be used, this again stresses the importance of the differential analysis as any systematic errors arising from using unblanketed models will not affect the differential analysis. In the case of OB 48-234 the Si II/Si III ionisation balance was utilised due to the absence of the Si IV line in the observed spectrum.

The quality of the fits for the hydrogen line profiles is illustrated in Fig. 5. The surface gravity is based on the fitting of the profile wings as the line cores are contaminated by both non-LTE effects and by wind emission (see Sect. 5). Both the H δ and H γ features are significantly blended with metal lines. Hence more weight was given to the long wavelength part

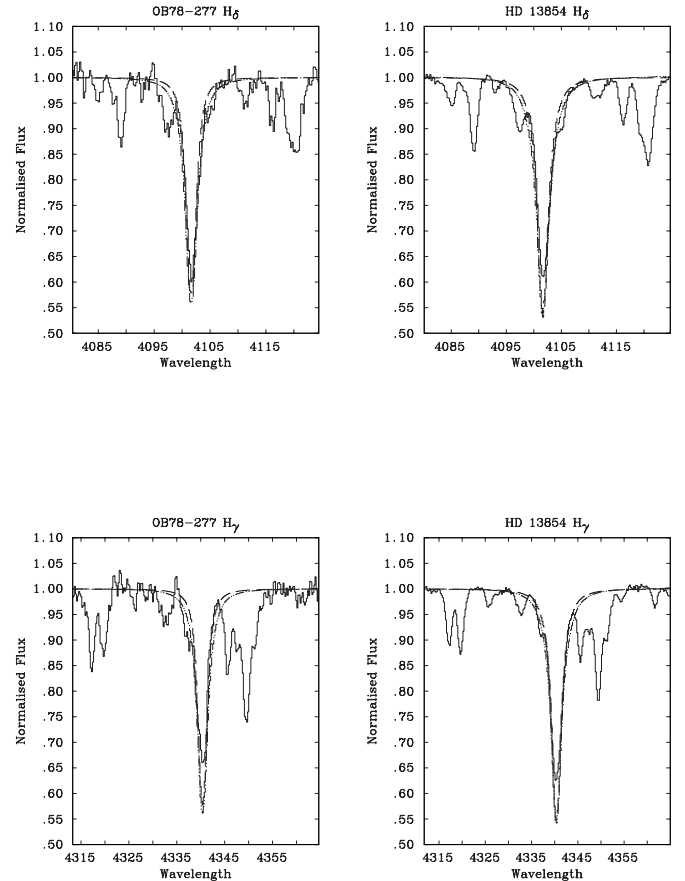


Fig. 5. The H δ and H γ profiles for OB 78-277 and its Galactic counterpart, HD 13854. In the case of OB 78-277 the theoretical profiles have surface gravities of $\log g = 2.5$ and 2.6 , whereas for HD 13854 the theoretical profiles are for $\log g = 2.6$ and 2.7 . The lower surface gravities are represented by the dashed (---) lines and the higher surface gravities by the dot-dot-dashed (⋯) lines. The observed spectra are represented by the solid lines.

of the profile in the former case and to the short wavelength part of the profile in the latter case. The equivalent widths of the silicon and hydrogen lines in the Galactic standards and M 31 supergiants are shown in Tables 2 and 3.

Microturbulence, ξ , also needs to be included in the iterative process to determine the atmospheric parameters. This parameter is introduced to ensure no variation of abundance with line strength within a particular ionic species. The microturbulent velocity of each star in the sample was determined from both the O II and Si III lines. Although O II has the richest line spectrum in these early B-type stars, with ~ 20 unblended lines in the program stars and ~ 35 in the Galactic standards, the scatter in abundances from one multiplet to another, due to errors in the atomic data and possible non-LTE effects, makes it difficult to constrain the appropriate value of microturbulence. On the other hand, the Si III multiplet at 4560 \AA has three lines covering a significant range in line strength and being from the same multiplet the abundances derived from these silicon lines should be less affected by such uncertainties than the oxygen lines. Hence the microturbulent velocities listed in Table 4 are derived from the silicon lines. It is interesting to note that

Table 2. Details of the Galactic comparison stars. Spectral types have been taken from Lennon et al. (1992), whilst the silicon and hydrogen line equivalent widths have been measured from our spectra.

Star name	Spectral Type	Si II			Si III		Si IV	H δ	H γ
		4128 Å	4130 Å	4552 Å	4568 Å	4574 Å	4116 Å		
HD 167264	O9.7Iab	225	200	100	435	1680	1690
HD 37128	B0Ia	304	243	113	489	1630	1560
HD 38771	B0.5Ia	376	314	182	357	1810	1810
HD 2905	BC0.7Ia	395	350	219	228	1360	1440
HD 13854	B1ab	456	390	241	135	1600	1640
HD 14956	B1.5Ia	494	426	280	94	1390	1470
HD 190603	B1.5Ia+	42	72	485	438	293	114	1130	1170
HD 14143	B2Ia	463	394	248	51	1320	1280
HD 14818	B2Ia	428	368	224	49	1550	1570
HD 194279	B2Ia	468	415	272	69	1130	1260

Table 3. Silicon and hydrogen line equivalent widths for the M 31 targets.

Star name	Si II			Si III		Si IV	H δ	H γ
	4128 Å	4131 Å	4552 Å	4568 Å	4574 Å	4116 Å		
OB 8-17	476	392	241	116	1350	1370
OB 8-76	391	341	256	414	1780	1600
OB 10-64	245	240	120	400	1690	1580
OB 48-234	97	126	457	426	240	...	1620	1500
OB 48-358	404	284	300:	221:	1600	1580
OB 78-159	293	237	119:	141	1640	1540
OB 78-277	473	438	269	164	1470	1380
OB 78-478	487	466	316	101	1650	1750

in all cases the microturbulent velocities determined from the O II lines were in the range of 5–7 km s⁻¹ larger than those derived from the Si III multiplet. This effect has also been observed in non-LTE analyses of early B-type giants and supergiants by Vrancken et al. (1998) and MLD, respectively.

As can be seen from Table 4 the microturbulence determined for both the M 31 and Galactic supergiants are in the range of 19 to 35 km s⁻¹, indicating supersonic velocities. For the Galactic standards, they are on average 15 km s⁻¹ greater than the values determined by MLD in their non-LTE analysis of the same sample. This discrepancy in microturbulence from LTE and non-LTE analyses has also been observed by Gies & Lambert (1992), in a sample of 5 supergiants. Since adopting a non-LTE analysis reduces the value of ξ , the large value we observe is probably due to departures from LTE (see Smartt et al. 1997). It may also be due to the presence of a macroscopic velocity field which can mimic microturbulence (see Kudritzki et al. 1992). However, as the effect is seen in both program and standard stars the differential abundances should still be reliable.

In the case of OB 48-358, only an upper limit in the equivalent width of Si III 4574 Å was obtained thus the microturbulence could not be derived from the Si III multiplet. However, we have adopted the same microturbulence as that of its standard HD 2905, $\xi = 21$ km s⁻¹, this is in close agreement to that derived from the O II lines of OB 48-358, which is 20 ± 7 km s⁻¹.

The projected rotational velocity, $v \sin i$, can be estimated when analysing supergiant spectra. This line broadening parameter was determined from a selection of seven unblended metal lines by fitting theoretical profiles to the observed spectra. The theoretical profiles were convolved with a Gaussian profile to account for the instrumental broadening. The profile is then convolved with a rotational line profile Fourier transform function, this has been described in detail by Gray (1976) and more recently by Rucinski (1990). It should be noted that the spectra of early B-type supergiants appear to show significant broadening (see, for example, Howarth et al. 1997). Hence, these estimates probably reflect the effects of both rotation and turbulence. The rotational velocity estimates are listed in Table 4 along with the adopted values for the above mentioned atmospheric parameters.

4.2. Chemical composition

In this section we will present the results of the LTE abundance analysis for seven of the M 31 B-type supergiants and discuss the abundances of individual elements. Although it was possible to make an approximate estimate of the effective temperature and surface gravity of OB 78-159, its composite nature excludes it from a quantitative abundance analysis and it is therefore omitted from any further discussion. The quality of the OB 8-76 spectrum was such that a differential abundance analysis was possible, and the results appear to be consistent

Table 4. LTE atmospheric parameters and galactocentric distances for both the M 31 and Galactic standard stars. The random errors in the atmospheric parameters are $\Delta T_{\text{eff}} = \pm 1000$ K; $\Delta \log g = \pm 0.2$ dex; $\Delta \xi = \pm 5$ km s⁻¹; $\Delta v \sin i = 15$ km s⁻¹. Also included is the degree of CN processing in the stars, the classifications are taken from MLD as are the designations for the Galactic standards. The status of the M 31 stars are discussed in Sect. 6.1. (× - “normal/moderate”; ○ - “processed?”; ● - “highly-processed”). The galactocentric distances of the Galactic standards are taken from Humphreys (1970).

Star name	T_{eff} (K)	$\log g$ (dex)	ξ	$v \sin i$ (km s ⁻¹)	R_g (Kpc)	Processing
M 31 Stars						
OB 8-17	22 000	2.5	32	72	5.85	●
OB 8-76	27 500	3.0	19	79	6.12	○
OB 10-64	30 500	3.4	21	...	5.90	○
OB 48-234	*21 500	2.5	27	64	11.41	×
OB 48-358	26 000	2.9	21	70	11.59	×
OB 78-159	26 000	3.0	9.50	
OB 78-277	23 000	2.5	24	73	9.58	○
OB 78-478	20 500	2.4	24	86	9.06	●
Galactic Standards						
HD 167264	31 500	3.5	20	...	8.73	○
HD 38771	29 500	3.2	25	90	10.37	○
HD 2905	25 500	2.8	21	79	10.48	×
HD 13854	23 000	2.6	27	64	11.30	●
HD 190603	21 000	2.3	28	70	9.69	●
	*21 500	2.3	23	70		
HD 14956	20 500	2.3	30	85	11.33	●
HD 14818	18 000	2.2	35	63	11.59	●

* The effective temperature for this star is determined from the Si II/Si III ionisation stages rather than the Si III/Si IV.

Table 5. LTE absolute elemental abundances for the M 31 B-type supergiants given as $\log\left[\frac{X}{H}\right] + 12$ (where X = element). The errors represent the standard deviation of the mean.

Ion	OB 8-17	OB 8-76	OB 10-64	OB 48-234	OB 48-358	OB 78-277	OB 78-478
He I	10.28 ± 0.28	11.50 ± 0.17	11.44 ± 0.22	10.97 ± 0.23	11.12 ± 0.33	10.89 ± 0.32	11.08 ± 0.37
C II	7.45	<7.80	8.09	7.68	<7.36	7.50	<7.69
N II	8.24 ± 0.19	8.92 ± 0.35	8.13	8.19 ± 0.16	<7.69	8.09 ± 0.13	8.51 ± 0.18
N III	...	8.31	8.36 ± 0.21
O II	8.44 ± 0.17	9.07 ± 0.26	8.74 ± 0.24	8.52 ± 0.22	8.66 ± 0.44	8.78 ± 0.38	9.02 ± 0.24
Mg II	7.60	<8.39	7.62	7.61	<7.37	7.53	7.42
Al III	7.35	<7.76	...	7.24	<7.66	6.97	7.68
Si II	7.50 ± 0.03
Si III	7.26 ± 0.01	8.17 ± 0.03	8.04 ± 0.10	7.47 ± 0.10	7.42 ± 0.17	7.49 ± 0.06	7.90 ± 0.07
Si IV	7.34	8.29	7.96	7.33	7.47	7.43	7.89
S III	6.99 ± 0.08	7.53	...	7.08	<6.92	6.91	7.36 ± 0.23
Fe III	7.28	<6.98	7.22

and reasonable. However they should be treated with caution as in the light of its peculiar radial velocity this target may be a binary.

As mentioned at the beginning of Sect. 4, we will concentrate on the results of differential abundance analysis rather than the absolute analysis, the results of which can be seen in Tables 5 and 6. For the differential analysis we attempted to fulfill certain criteria in selecting the appropriate standards for each target. The criteria were: 1) To match, as closely as

possible, the atmospheric parameters and spectral type, 2) To only use those stars that had unprocessed atmospheres according to MLD. Although it was possible to fulfill the first of our criteria for all cases, the second criterion was more difficult to adhere to, with it only being possible for OB 48-358. In the cases of the four other targets only Galactic supergiants which were described by MLD as “highly processed”, have similar atmospheric parameters. According to MLD, the identifier “highly processed” represents a supergiant with a

Table 6. LTE line-by line differential elemental abundances for the M 31 supergiants given as $\Delta \log[\frac{X}{H}] = \log[\frac{X}{H}]_* - \log[\frac{X}{H}]_{\text{standard}}$. The Galactic standards that were used in the differential analysis are listed in brackets under the appropriate M 31 star.

Ion	OB 8-17 (HD 13854)	OB 8-76 (HD 38771)	OB 10-64 (HD 167264)	OB 48-234 (HD 190603)	OB 48-358 (HD 2905)	OB 78-277 (HD 13854)	OB 78-478 (HD 14956)
He I	-0.12 ± 0.28	+0.34 ± 0.46	+0.04 ± 0.20	-0.06 ± 0.14	+0.05 ± 0.23	-0.18 ± 0.30	-0.05 ± 0.13
C II	+0.20	<0.20	-0.14	+0.41	< -0.08	+0.21	<0.33
N II	+0.16 ± 0.12	+0.72 ± 0.36	-0.09	-0.24 ± 0.30	<0.09	+0.02 ± 0.09	+0.05 ± 0.21
N III	...	+0.30	-0.04 ± 0.29
O II	-0.05 ± 0.14	+0.42 ± 0.25	-0.02 ± 0.22	-0.10 ± 0.43	-0.08 ± 0.47	+0.21 ± 0.19	+0.51 ± 0.37
Mg II	+0.15	<0.40	-0.01	-0.02	< -0.17	+0.08	+0.03
Al III	+0.16	<0.55	...	+0.07	<0.45	-0.24	+0.39
Si II	-0.08 ± 0.09
Si III	-0.04 ± 0.02	+0.45 ± 0.02	-0.15 ± 0.09	-0.16 ± 0.07	-0.23 ± 0.26	+0.19 ± 0.05	+0.36 ± 0.07
Si IV	-0.01	0.62	-0.21	-0.25	+0.03	+0.08	+0.40
S III	-0.06 ± 0.02	+0.13	...	+0.05	< -0.11	-0.15	+0.12 ± 0.15
Fe III	+0.41	< -0.07	+0.32

photosphere contaminated by the products of CN-cycle burning and so should exhibit a significant nitrogen enhancement with a lesser carbon depletion. In Sect. 6.1, we will discuss the effect that the possible contamination of the photospheres of our standards has on our analysis.

Helium: The helium abundance was determined from the non-diffuse He I lines at 3965, 4121 and 4713 Å which were well observed features in most of our M 31 targets. However for the cooler stars the 4121 Å line tended to be blended with metal lines making the line strengths difficult to determine. Weak features were observed in OB 8-17 and OB 48-234 at 4437 Å, while a weak line was also observed in OB 8-17 at 4169 Å. In addition to the non-diffuse lines, helium abundances were determined from the diffuse lines, this was done using profile fitting techniques. In all cases the results from the diffuse and non-diffuse helium lines were consistent. From Table 6 we see that the helium abundance of each of these stars is consistent with that of the standard stars, *within the errors*.

Carbon & nitrogen: The carbon abundances are determined from the close doublet at 4267 Å. This feature is known to be difficult to model in both LTE and non-LTE and hence the absolute abundances from this line should be treated with caution (see Lennon 1983; Eber & Butler 1988; Sigut 1996; MLD). The C II 4267 Å feature in OB 8-17 appeared to be affected by noise which may account for it having a larger abundance than its Galactic counterpart. Unlike carbon, nitrogen has a relatively rich spectrum in the M 31 stars except for the hotter stars OB 8-76 and OB 48-358 where the lines 3995 Å, 4236 Å and 4241 Å are the best observed lines. These two elements are important for identifying which stars have nucleosynthetically processed material mixed to their stellar surface.

Oxygen: This element has the richest spectrum in these early B-type supergiants and is a powerful diagnostic tool for determining the abundance gradient of M 31 (see Sect. 6).

Silicon: As discussed previously in Sect. 4.1, Si III & Si IV were used to determine the atmospheric parameters. The Si IV abundances presented in Table 5 are based on the 4116 Å line except for in the case of OB 48-234, where this line was unobserved in the spectrum. The Si IV abundance

of OB 48-234 is based on the 4088 Å line. The absolute abundances derived from the 4088 Å line in the other six stars tended to be larger than that from the 4116 Å line. Although blending with a nearby O II line was taken into account when measuring the equivalent width of this silicon line there is evidently still some contribution from this oxygen feature.

Magnesium, sulphur, aluminium: The magnesium abundances are based on a single feature, this is the close doublet at 4481 Å. This feature was well observed in most of the targets except OB 8-76 & OB 48-358, where it was only possible to determine upper limits. From the differential analysis the magnesium abundance in the target stars appear to be similar to that of the standards. The close doublet of Al III at 4529 Å is the only unblended aluminium feature in these early B-type supergiants. Again only upper limits could be derived for both OB 8-76 & OB 48-358. The sulphur abundance is determined from the S III feature at 4285 Å, where only an upper limit could be determined for OB 48-358. In the cooler stars of the sample OB 8-17 and OB 78-478 an additional S III feature was observed at 4361 Å.

Iron: The iron abundance was derived from a single Fe III feature at 4419 Å. This feature was only observed in the cooler stars of the sample OB 8-17, OB 48-234 & OB 78-478. From Table 6 it seems that iron is overabundant in OB 8-17 & OB 78-478. However this feature is relatively weak and in the standard spectra is affected by a diffuse interstellar absorption band. Hence this enhancement may not be significant.

5. Non-LTE model atmosphere and abundance analyses

A criticism to taking the LTE approach when analysing supergiants is that the derived abundances may be subjected to significant non-LTE effects. In order to investigate the uncertainties incurred in adopting a LTE analysis we have also carried out a non-LTE analysis on one of the M 31 supergiants and its Galactic standard. Given the relatively high signal-to-noise of OB 78-277, it was decided to carry out the non-LTE analysis for this star and its Galactic counterpart, HD 13854.

Table 7. Non-LTE atmospheric parameters for OB 78-277 and its Galactic standard, HD 13854. Wind parameters of OB 78-277 are adopted to be identical with those of HD 13854.

Parameter		OB 78-277	HD 13854
T_{eff}	(K)	21 000	21 000
$\log g$	(dex)	2.4	2.4
ξ	(km s ⁻¹)	16	17
v_{∞}	(km s ⁻¹)	1000	1000
\dot{M}	(M_{\odot} yr ⁻¹)	0.3×10^{-6}	0.3×10^{-6}
β -parameter		3.00	3.00
R_*	(R_{\odot})	40.8	40.8

The non-LTE code used is that by Santolaya-Rey, Puls & Herrero (1997). This is a “unified model atmosphere” code, which includes spherical extension and stellar winds, although omits metal line-blanketing at the present stage (see Santolaya-Rey et al. 1997 for full details of code). This code calculates both the atmospheric structure and line profiles and has a similar philosophy to that of the line formation code DETAIL (Butler & Giddings 1985), i.e. the code is data driven. The code includes atomic data for hydrogen, helium, carbon, nitrogen, oxygen, magnesium and silicon. The atomic models and Stark broadening data implemented in the line formation of hydrogen and helium are described in full in Santolaya-Rey et al. (1997). In the case of silicon, nitrogen and oxygen the metal ion populations and line profiles were calculated using the atomic data of Becker & Butler (1988, 1989, 1990). The atomic data used for C II are from Eber & Butler (1988), and the Mg II data are from Mihalas (1972).

The effective temperature and surface gravity of OB 78-277 and its standard, HD 13854, were estimated using similar procedures to that discussed in Sect. 4.1 i.e. from the Si III/ Si IV ionisation balance and profile fitting of H δ & H γ . In Fig. 6, we have plotted theoretical profiles of H δ & H γ , for $\log g = 2.4$ over normalised observed spectra of OB 78-277 and HD 13854. From a comparison with Fig. 5, it is clear that the wings of the non-LTE profiles fit the data better than in the LTE profiles for both of the Balmer lines. The cores of the non-LTE theoretical profiles are not as deep as the LTE profiles and also fit the observed data more accurately. This is due to the treatment of the stellar wind in the non-LTE analysis.

The wind terminal velocity (v_{∞}) for HD 13854 was taken from Kudritzki et al. (1999), whereas the mass-loss rate (\dot{M}) and β -parameter were determined from the H α profile. The stellar radius was derived from the absolute magnitude, deduced from the apparent magnitude after adopting a distance modulus (Garmany & Stencel 1992), and the emergent flux of the model atmosphere (Kudritzki 1987). As the wind parameters of HD 13854 describe an intermediate density wind there is no contamination of the weak metallic lines which are formed deep enough in the stellar atmosphere to be hardly effected by the wind. We have therefore adopted the same values of \dot{M} , v_{∞} and β -parameter for OB 78-277 as that of its Galactic counterpart. The microturbulence and silicon abundance were determined simultaneously from the Si III multiplet at ~ 4560 Å. The atmospheric parameters of both OB 78-277 and HD 13854

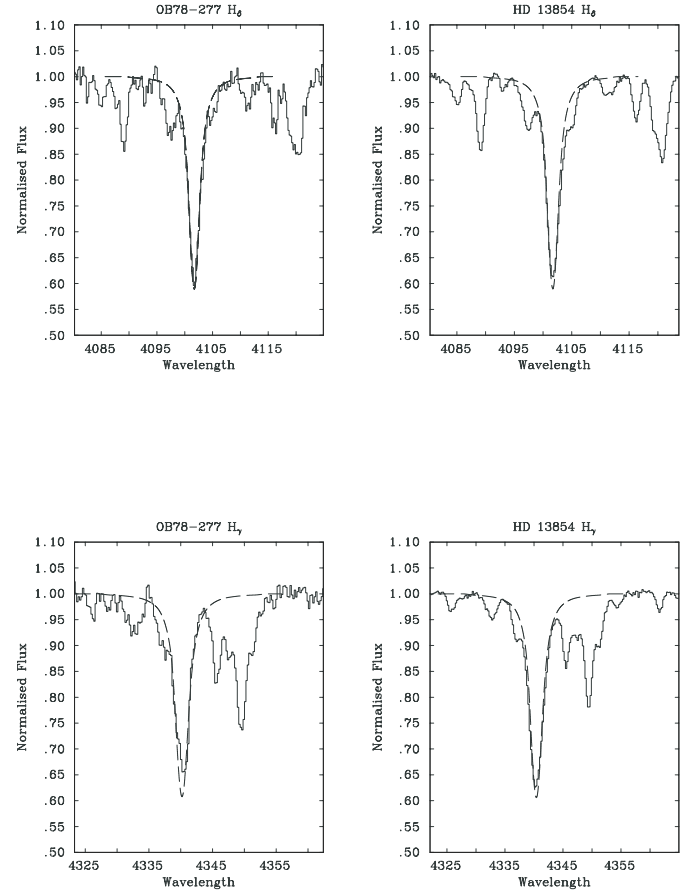


Fig. 6. The H δ and H γ profiles for OB 78-277 and its Galactic counterpart, HD 13854. The theoretical profiles have surface gravities of $\log g = 2.4$ and are represented by the dashed (---) lines. The observed spectra are represented by the solid lines.

are shown in Table 7. Adopting the microturbulence estimated from the Si III lines the abundances of carbon, nitrogen, oxygen and magnesium were obtained (see Table 8).

In Table 8 we present the non-LTE absolute and differential abundance results and include the LTE differential abundances, recalculated for the same lines as used in the non-LTE analysis. We can see the LTE and non-LTE *differential* abundance estimates differ by a maximum of ± 0.18 dex. This is reassuring as it is smaller than the uncertainties in our LTE abundance analysis and hence we can believe that the LTE differential analysis is not predominantly affected by non-LTE effects. Furthermore the difference in *absolute* oxygen abundances between the LTE and non-LTE analyses is 0.07 dex (see Tables 6 and 8), and therefore smaller than our estimated errors in the LTE analysis. In Fig. 8 we included the non-LTE oxygen abundance of OB 78-277, it is clear that if non-LTE effects of the same magnitude were present for the other B-type supergiants there would be no significant effect on the derived abundance gradient of M 31.

In Sect. 4 we have discussed the LTE analysis of OB 10-64 (see Table 5), this star has been analysed previously by Smartt et al. (2001b) using a non-LTE model atmosphere code. The model atmospheres generated by Smartt et al. (2001b) used the plane-parallel, non-line blanketed TLUSTY code of

Table 8. Non-LTE absolute and differential elemental abundances of OB 78-277 and its Galactic standard, HD 13854. Also included are the results of the LTE differential analysis for comparison. These have been recalculated using the same lines as used in the NLTE analysis only. $\Delta[\frac{X}{H}] = \log[\frac{X}{H}]_* - \log[\frac{X}{H}]_{\text{standard}}$.

ION	$12 + \log [\frac{X}{H}]$		$\Delta[\frac{X}{H}]$	
	OB 78-277	HD 13854	non-LTE	LTE
C II	7.76	7.56	+0.20	+0.21
N II	7.85 ± 0.14	7.95 ± 0.12	$+0.03 \pm 0.09$	-0.11 ± 0.05
O II	8.71 ± 0.08	8.33 ± 0.22	$+0.38 \pm 0.11$	$+0.23 \pm 0.10$
Mg II	7.55	7.65	-0.10	+0.08
Si III	7.42 ± 0.17	7.14 ± 0.05	$+0.28 \pm 0.02$	$+0.19 \pm 0.05$
Si IV	7.34	7.09	+0.25	+0.08

Hubeny (1988). For the line formation calculations the codes DETAIL (Giddings 1981) and SURFACE (Butler 1984) were used. It is reassuring to note that comparing the non-LTE differential analysis of OB 10-64 from Smartt et al. (2001b) to the LTE analysis included here, a maximum difference in the abundances of ± 0.18 dex is again observed. Moreover comparing the non-LTE absolute oxygen abundance of Smartt et al. (2001b) to the LTE abundance given in Sect. 4 a difference of 0.05 dex is found (see Fig 8).

In conclusion, the results of this section imply that the non-LTE effects on the abundances in these B-type supergiants appear to be less significant than the typical errors in our LTE analysis. Moreover, the results from the differential LTE analyses appear to be reliable indicators of the chemical composition in these M 31 supergiants.

6. Discussion

Here we first discuss the degree of processing in each of the M 31 supergiants followed by a comparison of the abundances determined in this analysis with those of previous nebular and stellar investigations. Finally the abundance gradient of M 31 will be discussed in detail.

6.1. Degree of chemical processing in the M 31 supergiants

Chemical peculiarities can be present in stellar photospheres due to mixing of core-processed material. Current models predict that if CNO-cycled material was mixed to the surface there would be an observed enhancement in helium and nitrogen accompanied by a depletion in carbon and oxygen (see Maeder & Meynet 1988; Gies & Lambert 1992; Meynet & Maeder 2000; Heger & Langer 2000). In a sample of 46 Galactic B-type supergiants MLD identified three sub-groups based on the amount of processing observed in the stellar photosphere: “normal/moderate”, “processed?” and “highly processed”. The first group could be associated with stars having chemically near normal photospheres whilst the latter is designated to stars which clearly show products of CN-cycled material in their photospheres. The “processed?” group may have some contamination from core material but of a lesser extent than the “highly-processed” stars. In their analysis MLD concluded that there was no obvious correlation between helium abundances

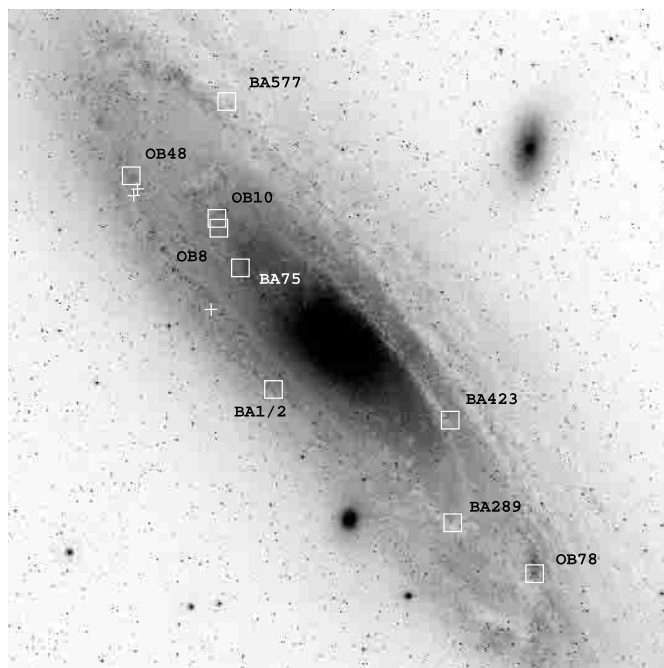


Fig. 7. Mosaic of DSS images of M 31 with the positions of associations OB 8, OB 10, OB 48 and OB 78 represented by squares. The image size is $90' \times 90'$ with north up and east to the left. The three pluses (+) are the A-type supergiants from VMLPKL in increasing order of DEC; 41-2368, 41-3712 & 41-3654. The F-supergiant (A-207) from the VMLPKL sample lies off the field-of-view in the outer south west corner of M 31. The H II regions from Blair et al. (1982) which fall in this $90' \times 90'$ image are displayed. The H II regions K315 & K703, of Galarza et al. (1999), have been omitted for clarity of the image. K315 is coincident with the OB 10 association, whereas K703 lies very close but not coincident with the OB 48 association.

and the assigned chemical sub-groups. However in the most luminous stars and those in the “highly processed” category oxygen had stronger features than the chemically normal supergiants. Thus no conclusive information on the correlation of oxygen with the degree of processing could be obtained.

By comparing the carbon and nitrogen line strengths and abundances of the M 31 supergiants to those of their Galactic counterparts and considering the labels assigned by MLD, we shall discuss to what degree the M 31 stars are processed, if at all. Smartt et al. (2001b) suggested that OB 10-64 belongs to the “processed?” sub-group, this is consistent with our findings.

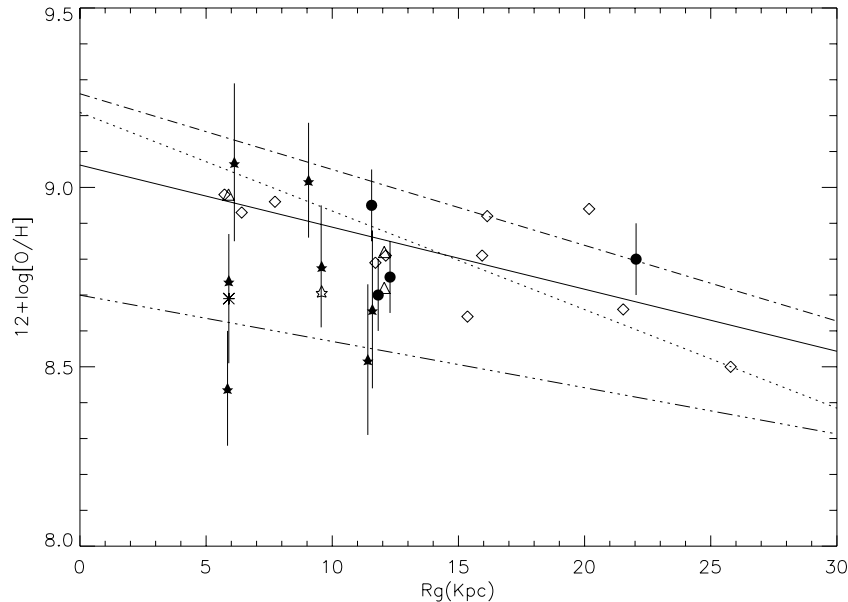


Fig. 8. Oxygen abundances for H II regions and supergiants in M31 as a function of galactocentric distances. The solid stars (★) are the abundance results of the seven B-type supergiants in this study. The unfilled star is the non-LTE oxygen abundance for OB 78-277. The asterisk (*) is the photospheric NLTE abundance of OB 10-64 from Smartt et al. (2001b). The open diamonds (◇) and open triangles (△) are the abundances of the H II regions from Blair et al. (1982) and Galarza et al. (1999), respectively, calculated using McGaugh (1991) calibrations. The solid circles (●) are the abundances of four A-F-type supergiants from VMLPKL. The dotted (· · ·), solid (-), dash-dot (- · -) and dash-dot-dot-dot(- · · ·) lines are the least squares fit through the H II regions of Blair using McGaugh (1991), Pagel et al. (1980), Zaritsky et al. (1994) and Pilyugin (2001a) calibrations, respectively. The error bars in the stellar results represent the standard error in the mean.

This star has similar carbon and nitrogen line strengths as that of the Galactic supergiant HD 167264, which has been classified as “processed?” by MLD.

As the standard for OB 48-358 is classified as “normal” the differential analysis is easier to interpret. OB 48-358 appears to be in the “normal/moderate” category as the C II 4267 & N II 3995 lines strengths are similar to that of the standard. Although the C II 4267 line of OB 8-76 is of similar line strength to that of its standard the N II is stronger indicating that “processed?” or “highly-processed” would be the appropriate classification. MLD plotted the N/C line strength ratios against the logarithmic effective temperature of their Galactic supergiants and found that there is a correlation between the degree of chemical processing and this parameter (see Fig. 9. MLD). From this plot it would appear that OB 8-76 is a member of the “processed?” sub-group. The two OB 78 supergiants appear to be either “processed?” or “highly processed”. In both stars the carbon line strengths are similar to their “highly processed” standards. For OB 78-277 the nitrogen is slightly weaker than that of its Galactic counterpart and from its line strength ratio it appears to be “processed?”, whilst all the evidence points to OB 78-478 being a member of the “highly processed” group. OB 8-17 appears to be as processed as HD 13584 if not slightly more as indicated from the N II 4630 Å line. As HD 13854 is in the “highly processed” sub-group OB 8-17 must also belong to this classification. In OB 48-234 carbon is stronger than the standard while nitrogen is weaker purely indicating that this star belongs to the “normal/moderate” group as the standard is “highly processed. These classifications are summarised in Table 4.

6.2. Comparison of B-type supergiants with previous results.

To compare the abundances of this set of supergiants with those of previous stellar studies, it is appropriate to discuss the composition of stars at similar galactocentric distances. Only one previous stellar investigation by VMLPKL has been carried out in M31 (the results of Smartt et al. 2001b have been subsumed into this paper). Two of their M31 A-type supergiants lie in close proximity to the OB 48 association at a galactocentric distance of approximately 11.5 kpc (see Figs. 7 and 8). The common elements observed in the A & B-type supergiants are Fe and the α -processed elements Si, O, Mg. It is important to note that the A-type supergiants were analysed using a non-LTE analysis, hence when comparing abundances between the A & B-type supergiants the uncertainties discussed in Sect. 5 must be considered. The α -processed element abundances in these A & B-type supergiants are in good agreement, *within the errors*. The OB 48 oxygen abundances are ~ 0.1 dex lower than those of the A-type supergiants but given the errors of both analyses, including the non-LTE effects, this difference is considered to be negligible. OB 48-234 has a marginal Fe III feature which gives a significantly lower Fe abundance than that observed in the A-type supergiants. However given that this feature is weak and that the iron abundances from OB 8-17 & OB 78-478 are similar to that of the A-type supergiants, no significance is given to this result.

From nebular studies only abundances of oxygen are available for comparison with our results. In addition to the two A-type supergiants near association OB 48, there are also two H II regions from the analysis of Galarza et al. (1999)

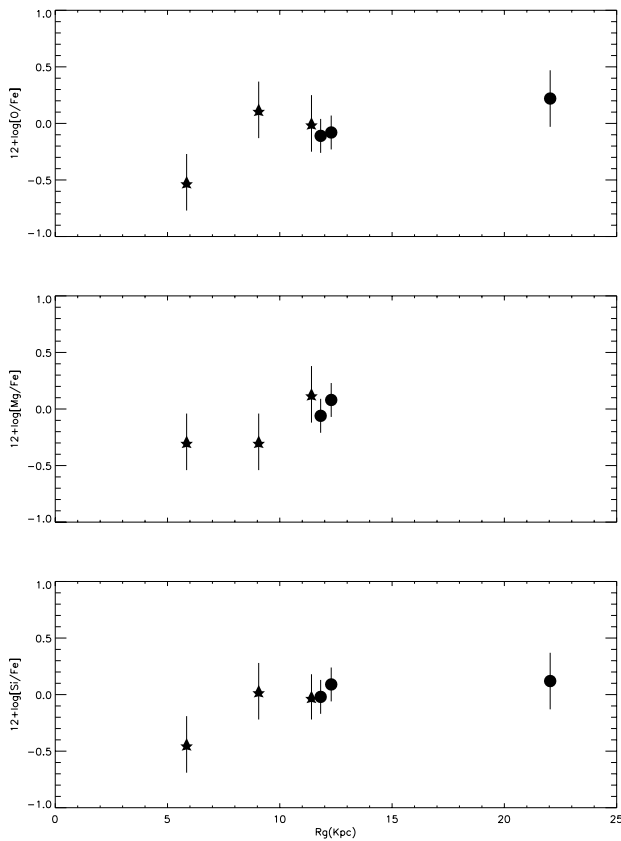


Fig. 9. The element ratios $\Delta[\text{O}/\text{Fe}]$, $\Delta[\text{Mg}/\text{Fe}]$ and $\Delta[\text{Si}/\text{Fe}]$ from our B-type supergiant sample (\star) and the A-F-type supergiants of VMLPKL (\bullet). Where $\Delta[\text{X}/\text{Fe}] = [\text{X}/\text{Fe}]_{\text{M31}} - [\text{X}/\text{Fe}]_{\text{Standard}}$, in the case of the B-type supergiants the standards are as those for the differential analysis (see Table 6), whereas for the A-F-type supergiants the sun was taken as a standard.

(K703 & K722). Unfortunately these H II regions are not spatially coincident with our targets. There appears to be a 0.2 dex difference in the oxygen abundances derived from the H II regions and those from the B-type supergiants, with the former having the higher abundances. However, this depends on the calibration of the line ratio parameter, R_{23} with $[\text{O}/\text{H}]$, and the various calibrations give a spread of ~ 0.2 dex in abundance. For example using the calibration of Mc Gaugh (1991), the magnitude of the difference in abundance between the two H II regions mentioned above and the OB 48 stars is 0.2 dex, whereas adopting the Zaritsky et al. (1994) calibration a difference of 0.36 dex is observed (see Fig. 8). Smartt et al. (2001b) also observed this difference in the abundances derived from these calibrations of the R_{23} parameter when comparing the abundances of OB10-64 to that of a spatially coincident H II region, K315 (Galarza et al. 1999). In contrast to this, VMLPKL found that there was good agreement of the oxygen abundances in H II regions with that of their A-type supergiant sample.

The above mentioned calibrations of the R_{23} with $[\text{O}/\text{H}]$ all have a systematic error inherent in their results, as they have not considered the physical conditions (i.e. the hardness of the ionizing radiation and the geometrical conditions) of the H II regions (for further details see Pilyugin 2000). A more recent

Table 9. Comparison of the oxygen abundance gradients derived from the H II region data of Blair et al. (1982) using four different calibrations, and the stellar results from A and B-type supergiants.

Element	Data	Calibration	Gradient (dex kpc ⁻¹)
Oxygen	H II regions	McGaugh	-0.027 ± 0.01
Oxygen	H II regions	Zaritsky et al.	-0.021 ± 0.01
Oxygen	H II regions	Pagel et al.	-0.017 ± 0.01
Oxygen	H II regions	Pilyugin	-0.013 ± 0.01
Oxygen	B-type stars	This paper	-0.006 ± 0.02
Magnesium	B-type stars	This paper	-0.023 ± 0.02
Silicon	B-type stars	This paper	-0.009 ± 0.02

calibration by Pilyugin (2001a, 2001b), known as the *P*-method, considers the physical conditions of the H II regions by introducing an excitation index, *P*. This excitation index has a correlation with the effective temperature of the ionizing star and hence is a good indicator of the hardness of the ionizing radiation. The oxygen abundances derived for the M 31 H II regions using this *P*-method are significantly less (~ 0.3 – 0.5 dex) than those derived using the calibrations of Mc Gaugh (1991) & Zaritsky et al. (1994) and are in better agreement with the oxygen abundances of the B-type supergiants in our sample. Furthermore using this calibration a solar oxygen abundance is indicated for the center of M 31 (see Fig. 8).

6.3. Abundance gradients and ratios of M 31

The form of the abundance gradient in M 31 is still open to debate. Nebular studies in recent years have suggested that a shallow abundance gradient is present in M 31, whereas the one stellar investigation (of just three stars) does not show a clear gradient (Blair et al. 1982; Galarza et al. 1999; VMLPKL).

Taking the set of 11 H II regions of Blair et al. (1982), we have plotted the oxygen abundance as a function of the M 31 galactocentric distance (see Fig. 8). The plotted data points (open diamonds, \diamond) are those derived using the calibration of Mc Gaugh (1991), with the galactocentric distances recalculated for the latest value of the distance to M 31; 783 ± 30 kpc from Holland (1998). The least-squares fit to these data points gives an oxygen abundance gradient of -0.027 dex kpc⁻¹ and implies from extrapolation a central oxygen abundance of 9.21 dex. Also plotted in Fig. 8 are the least-squares fit to the nebular oxygen abundances adopting the calibrations of Zaritsky et al. (1994), Pagel et al. (1980) and Pilyugin (2001a). These imply shallower gradients of -0.021 dex kpc⁻¹, -0.017 dex kpc⁻¹ and -0.013 dex kpc⁻¹ and central oxygen abundances of 9.20 dex, 9.06 dex and 8.70 dex, respectively. These results are summarised in Table 9 for easy comparison with the B-supergiant results.

The least-squares fit to our sample of supergiants within 12 kpc of the galactic center suggests an abundance gradient consistent with that derived from the nebular results, -0.017 ± 0.02 dex kpc⁻¹. However as OB 8-76 is possibly a multiple system, this result should be omitted from our abundance gradient analysis. This then gives a negligible oxygen abundance

gradient in M 31 of $-0.06 \pm 0.02 \text{ dex kpc}^{-1}$. Furthermore negligible abundance gradients are also derived from the average silicon abundances in each of the four OB associations. However from the magnesium abundances in each association an abundance gradient of $-0.023 \pm 0.02 \text{ dex kpc}^{-1}$ is observed. VMLPKL also investigated the radial oxygen abundance gradient of M 31, unlike the nebular results, they found that there is no gradient between 10 kpc and 20 kpc. However as the VMLPKL study has abundances from only three objects over a fairly narrow galactocentric range, one must take this as a very preliminary result.

As discussed in Sect. 6.1 variations in the photospheric abundances of carbon, nitrogen and oxygen from their initial values have been predicted by stellar evolutionary models of blue supergiants, such as those based on stellar rotation (see Meynet & Maeder 2000; Heger & Langer 2000). However these models predict that only very small changes in the oxygen abundance will have taken place by the end of the main-sequence ($\sim 10\%$ by number). Moreover such a depletion in oxygen has not been observationally proven in B-type supergiants which have highly processed photospheres (for example see MLD). If there is a change in oxygen of the magnitude predicted by these models it is masked by the uncertainties in our observations and therefore would not effect the oxygen abundance gradient. Reassuringly, the silicon and magnesium gradients are consistent with that of the oxygen abundance gradient and these elements should not be effected by the products of CNO-cycle burning.

The O, Mg, Si & S abundances of OB 8-17, the innermost star of our sample, are comparable to those of its Galactic counterpart; HD 13854. This is also the case for the nearby star OB 10-64, as its O, Mg and Si abundance are very similar to that of the standard star HD 167264. This implies that unlike the common opinion that the center of M 31 is metal rich, as indicated by nebular results (Blair et al. 1982; Galarza et al. 1999), it appears to be of solar metallicity. This was suggested by Smartt et al. (2001b) from their NLTE analysis of OB 10-64 and is consistent with the nebular results calculated using the *P*-method calibration of Pilyugin (2001a, 2001b).

At this point it is worthwhile discussing the element ratios $[\text{O}/\text{Fe}]$, $[\text{Mg}/\text{Fe}]$ & $[\text{Si}/\text{Fe}]$ in M 31. The ratio of these α -processed elements to iron can indicate the star formation history of M 31 due to the different nucleosynthetic origins of these elements. The bulk of iron production is thought to come from low and intermediate mass stars in degenerate binary systems during explosions of Type Ia supernovae, whereas the α -processed elements are mainly produced in massive stars which enrich the ISM through core-collapse Type II supernovae. VMLPKL observed an increase in $\Delta[\text{O}/\text{Fe}]$ toward the outer disk of M 31, and noted a possible increase in $\Delta[\alpha/\text{Fe}]$, excluding oxygen. In Fig 9 we plot the element ratios $\Delta[\text{O}/\text{Fe}]$, $\Delta[\text{Mg}/\text{Fe}]$ & $\Delta[\text{Si}/\text{Fe}]$ against galactocentric distance for our target sample and for that of VMLPKL. Consistent with the findings of VMLPKL, there is evidence for an increasing gradient in each of these elements.

7. Conclusion

We have presented the results of detailed LTE absolute and differential abundance analyses of the largest group of B-type supergiants in M 31 studied to date. Non-LTE calculations have also been carried out to investigate the effect of departures from LTE on our results. It was shown that although analysed using LTE model atmospheres and line formation codes the analysis is dominated by uncertainties stemming from the quality of the data rather than non-LTE effects.

The seven B-type supergiants lie in distinct clusters which cover a galactocentric distance of 5–12 kpc and from the derived abundances we estimated the oxygen abundance gradient of M 31. Across this fairly restricted range of the disk we do not find any evidence of a significant abundance gradient, which is similar to the result found by VMLPKL for four A-F -type supergiants. Radial abundance gradients for the α -processed elements, Si & Mg, were also determined indicating a negligible silicon abundance gradient and a possible shallow gradient for magnesium. However we emphasize that we still have a very restricted number of data points with which to probe the abundance gradient in M 31. The work of Smartt & Rolleston (1997), in determining abundance gradients in the Milky Way, cautions against using small numbers of stars with restricted Galactocentric radii to draw firm conclusions on existence of abundance gradients. This result is reasonably consistent with the shallow negative oxygen abundance gradients determined from H II regions and supernovae remnants (Dennefeld & Kunth 1981; Blair et al. 1982; Galarza et al. 1999).

It has been shown that dependent on which empirical calibration of the R_{23} parameter with $[\text{O}/\text{H}]$ that is adopted, different magnitudes of the radial abundance gradient in M 31 are obtained. It has also been shown that there is an offset between the abundances obtained from the H II regions and that of the B-type supergiants ($\sim 0.15\text{--}0.4 \text{ dex}$), at the same galactocentric distance, which again depends on the empirical calibration implemented. These results indicate that the calibration of the R_{23} parameter with $[\text{O}/\text{H}]$ for H II regions with high metallicity/low excitation are clearly not accurately constrained. The empirical calibration which fits our stellar results best is that of Pilyugin (2000, 2001a, 2001b). Moreover this calibration gives the shallowest oxygen abundance gradient ($\sim 0.013 \text{ dex kpc}^{-1}$). The main difference between this and other calibrations is that it considers the hardness of the ionising radiation and therefore the physical parameters of the H II regions. As the B-supergiants only probe out to 12 kpc from the centre of M 31, it would be highly desirable to sample the outer regions of the M 31 disk with similar stars.

Our results for the innermost supergiants of the sample, OB 8-17 & OB 10-64, indicate that M 31 is not metal-rich, as previously thought from the results of H II regions, but actually suggests that it is of solar metallicity. This is consistent with the results obtained by Smartt et al. (2001b) and from the nebular oxygen abundances when implementing the empirical calibration of Pilyugin (2000, 2001a, 2001b). Although the star OB 8-76 appears to have quite high abundances, the

mean abundance of the OB 8 cluster is not significantly above the solar neighbourhood.

Smartt et al. (2001b) have shown that detailed wind-analyses can be accurately carried out on B-type supergiants in M 31. They also found that the wind momentum-luminosity relation of Kudritzki et al. (1999) can be applied to these B-type supergiants. In the future to calibrate the WLR for the metallicity of M 31 and further the calibration of WLR in the Local Group, the atmospheric parameters and abundances will be used in conjunction with the terminal velocity (see Bresolin et al. 2002) and mass-loss rates of the wind. The final aim of this work will be to provide an accurate and independent extragalactic distance scale.

Acknowledgements. We are grateful to the continuous support from A. Herrero of the IAC, Spain. We thank J. Puls for providing the non-LTE “unified model atmosphere” code. CT is grateful to the Department of Higher and Further Education, Training and Employment for Northern Ireland (DEFHTE) and the Dunville Scholarships fund for their financial support. PLD is grateful to the UK Particle Physics & Astronomy Research Council (PPARC) for financial support. SJS also thanks PPARC for financial support in the form of an Advanced Fellowship award. The WHT is operated on the island of La Palma by the Isaac Newton Group in the Spanish Observatorio del Roque de los Muchachos of the Instituto de Astrofísica de Canarias.

References

- Becker, S. R., & Butler, K. 1988, *A&A*, 201, 232
 Becker, S. R., & Butler, K. 1989, *A&A*, 209, 244
 Becker, S. R., & Butler, K. 1990, *A&A*, 235, 326
 Berkhuijsen, E. M., Humphreys, R. M., Ghigo, F. D., & Zumach, W. 1988, *A&AS*, 76, 65
 Blair, W. P., Kirshner, R. P., & Chevalier, R. A. 1982, *ApJ*, 254, 50
 Bresolin, F., Kudritzki, R. P., Lennon, D. J., et al. 2002, *ApJ*, in press
 Butler, K. 1984, Ph.D. Thesis, University of London
 Butler, K., & Giddings, J. R. 1985, Coll. Comp. Project No. 7 (CCP7), Newsletter 9, London, p. 7
 Cunha, K., & Lambert, D. 1994, *ApJ*, 426, 170
 Dennefeld, M., & Kunth, D. 1981, *AJ*, 86, 989
 Eber, F., & Butler, K. 1988, *A&A*, 202, 153
 Galarza, V. C., Walterbos, R. A. M., & Braun, R. 1999, *AJ*, 118, 2775
 Garmy, C. D., & Stencel, R. E. 1992, *A&A*, 202, 153
 Giddings, J. R. 1981, Ph.D. Thesis, University of London
 Gies, D. R., & Lambert, D. L. 1992, *ApJ*, 317, 724
 Gray, D. F. 1976, *The observation and analysis of stellar photospheres* (Cambridge university press) 2nd ed.
 Heger, A., & Langer, N. 2000, *ApJ*, 544, 1035
 Holland, S. 1998, *PASP*, 110, 759
 Howarth, I. D., Murray, J., Mills, D., & Berry, D. S. 1996, *STARLINK User Note SUN 50*, Rutherford Appleton Laboratory/CCLRC
 Howarth, I. D., Siebert, K. W., Hussain, G. A. J., & Prinja, R. A. 1997, *MNRAS*, 284, 265
 Hubeny, I. 1988, *Computer Physics Comm.*, 52, 103
 Humphreys, R. M. 1970, *AJ*, 75, 620
 Kobulnicky, H. A., Kennicutt, R. C., & Pizagno, J. L. 1999, *ApJ*, 514, 544
 Kudritzki, R. P. 1987, *A&A*, 174, 183
 Kudritzki, R. P. 1992, *A&A*, 266, 395
 Kudritzki, R. P., Puls, J., Lennon, D. J., et al. 1999, *A&A*, 350, 970
 Kudritzki, R. P., & Puls, J. 2000, *ARA&A*, 38, 613
 Kurucz, R. L. 1991, in *Precision Photometry: Astrophysics of the Galaxy*, ed. A. G. Davis-Philip, A. R. Uggren, & P. L. Janes (Schenectady: Davis)
 Lennon, D. J. 1983, *MNRAS*, 205, 829
 Lennon, D. J., Dufton, P. L., & Fitzsimmons, A. 1992, *A&AS*, 94, 569
 Lennon, D. J. 1997, *A&A*, 317, 871
 Maeder, A., & Meynet, G. 1988, *A&AS*, 76, 411
 Massey, P., Armandroff, T. E., & Conti, P. S. 1986, *AJ*, 92, 1303
 Massey, P., Armandroff, T. E., Pyke, R., et al. 1995, *AJ*, 110, 2715
 McCarthy, et al. 2002, in prep.
 McErlean, N. D., Lennon, D. J., & Dufton, P. L. 1999, *A&A*, 349, 553
 McLaugh, S. S. 1991, *ApJ*, 380, 140
 Meynet, G., & Maeder, A. 2000, *A&A*, 361, 101
 Mihalas, D. 1972, *ApJ*, 177, 115
 Monteverde, M. I., Herrero, A., & Lennon, D. J. 2000, *ApJ*, 545, 813
 Pagel, B. E. J., Edmunds, M. G., & Smith, G. 1980, *MNRAS*, 193, 219
 Peters, G. J. 1976, *ApJS*, 30, 551
 Pilyugin, L. S. 2000, *A&A*, 362, 325
 Pilyugin, L. S. 2001, *A&A*, 369, 594
 Pilyugin, L. S. 2001, *A&A*, 373, 56
 Puls, J., Kudritzki, R. P., Herrero, A., et al. 1996, *A&A*, 305, 17
 Rolleston, W. R. J., Hambly, N. H., & Dufton, P. L. 1997, *MNRAS*, 290, 422
 Rubin, V. C., & Ford, W. K. 1970, *ApJ*, 159, 379
 Ruckinski, S. M. 1990, *PASP*, 102, 306
 Santolaya-Rey, A. E., Puls, J., & Herrero, A. 1997, *A&A*, 323, 488
 Sigut, T. A. A. 1996, *ApJ*, 473, 452
 Smartt, S. J., Dufton, P. L., & Rolleston, W. R. J. 1996a, *A&AS*, 116, 483
 Smartt, S. J., Dufton, P. L., & Rolleston, W. R. J. 1996b, *A&A*, 305, 164
 Smartt, S. J., & Rolleston, W. R. J. 1997, *ApJ*, 481, L47
 Smartt, S. J., Dufton, P. L., & Lennon, D. J. 1997, *A&A*, 326, 763
 Smartt, S. J., Venn, K. A., Dufton, P. L., et al. 2001, *A&A*, 367, 86
 Smartt, S. J., Crowther, P. A., Dufton, P. L., et al. 2001, *MNRAS*, 325, 257
 Unwin, S. C. 1983, *MNRAS*, 205, 773
 van der Bergh, S. 1964, *ApJS*, 9, 65
 Venn, K. A. 1995, *ApJS*, 99, 659
 Venn, K. A., McCarthy, J. K., Lennon, D. J., et al. 2000, *AJ*, 541, 610
 Vranken, M., Lennon, D. J., Dufton, P. L., & Lambert, D. L. 2000, *A&A*, 358, 639
 Zaritsky, D. 1992, *ApJ*, 390, L73
 Zaritsky, D., Kennicutt, R. C., & Huchra, J. P. 1994, 420, 872